Journal of The Electrochemical Society, **151** (11) A1804-A1809 (2004)
0013-4651/2004/151(11)/A1804/6/$7.00 © The Electrochemical Society, Inc.

Tin Nanoparticle Loaded Graphite Anodes for Li-Ion Battery Applications

Yong Wang,[a,*] Jim Y. Lee,[a,b,,z] and Theivanayagam C. Deivaraj[b,**]**

[a]*Department of Chemical and Biomolecular Engineering, National University of Singapore 119260, Singapore*
[b]*Singapore-MIT Alliance, National University of Singapore 117576, Singapore*

Nearly monosized Sn nanoparticles were produced by an *in situ* prepared single-source molecular precursor approach. The experimental conditions in the $NaBH_4$ reduction of (phen)$SnCl_4$ (phen = 1, 10 phenanthroline) in water were carefully controlled to produce two different particle size ranges, 2-5 nm (mean: 3.5 nm, standard deviation: 0.8 nm) and 7-13 nm (mean: 10.0 nm, standard deviation: 1.7 nm). The Sn nanoparticles were subsequently dispersed in graphite (KS6) and the application of the resulting nanocomposites as an active anode material for Li-ion batteries was explored. The graphite-Sn nanocomposites showed significant improvement in the cyclability of Sn over previously reported results. The cyclability improvement is believed to be due to the smallness of the Sn particles and their uniform distribution in a soft matrix (graphite) which, in addition to being a capable Li^+ host, could also effectively buffer the specific volume changes in Sn-based Li storage compounds during charging (Li^+ insertion) and discharging (Li^+ extraction) reactions.
 [DOI: 10.1149/1.1799491]

Manuscript submitted November 7, 2003; revised manuscript received April 6, 2004. Available electronically October 4, 2004.

The interest in Sn-based anodes for lithium ion batteries has not been dampened by the often cited disadvantages of these mateirals,[1-5] namely, the stress-induced pulverization of the electrode caused by the large specific volume changes in charging (Li^+ insertion) and discharging (Li^+ extraction) reactions. Recently Li and Martin reported excellent cyclability and unprecedented rate capability (>700 mAh/g at the 8 C rate) in a restricted potential range (0.2-0.9 V) for SnO_2 films with nanometer size microstructure.[6] Such outstanding work aside, the prevailing view in the battery community prefers to combine a moderate use of the high capacity Li storage compounds such as Sn with graphite, the ubiquitous anode material for Li-ion batteries. Such measures not only address the material problems of the high capacity anodes, but also alleviate the need to develop new processes for the conversion to a completely new anode material. The dispersion of small (particularly nanoscale) particles of Sn, SnO, SnO_2, and SnSb in a carbonaceous matrix also allows operation in a more extended potential range (~5 mV-2.0 V).[7-17] The particles must be stabilized or particle agglomeration would occur during applications to nullify the advantages of small particles.[15-17] The use of elemental Sn nanoparticles is preferred over SnO_2 nanoparticles as they can, in principle, eliminate the irreversible capacity loss associated with the decomposition of tin compounds in the first lithiation cycle. However, the preparation of nanosized Sn particles is difficult, and there have been only a few reports. The direct chemical reduction of $SnCl_2$ often results in particles bigger than 1 μm.[18] Chaudret and co-workers have described a method by which 15-25 nm tin particles were obtained from the thermolysis of $[Sn(NMe_2)_2]_2$.[19] The primary interest of that work lay, however, with the oxidation of the Sn nanoparticles to SnO_2 nanoparticles for gas sensor applications. The physical vapor deposition based techniques, while relatively more common, are nevertheless an expensive alternative to the chemical preparation of nanoscale Sn.[20,21]

This paper reports a very simple procedure for preparing Sn nanoparticles of average particle sizes of 3.5 and 10.0 nm through an *in situ* prepared single-source molecular precursor. 1,10-phenanthroline (phen) was used to form a coordinating compound with $SnCl_4$ which was subsequently reduced at room temperature to produce the nanoparticles. The chelating properties of phen are also instrumental for controlling particle growth and agglomeration processes. The Sn nanoparticles so prepared are stable and show no sign of agglomeration throughout the experiments. The nanoparticles were characterized by transmission electron microscopy (TEM), powder X-ray diffraction (XRD), UV-visible and Fourier transform infrared (FTIR) spectroscopies, and X-ray photoelectron spectroscopy (XPS). Sn-graphite nanocomposites were prepared by introducing graphitic carbon during the nanoparticle synthesis. The performance of the Sn-graphite nanocomposites as anodes in rechargeable Li batteries was evaluated by laboratory test cells. To the best of our knowledge, this is the best effort in preparing the most uniform and stable Sn nanoparticles. The electrochemical cyclability of the Sn-graphite nanocomposites is also superior to most Sn-C or SnX-C composite materials (SnX = SnO, SnO_2, or SnSb) reported to date.

Experimental

Chemicals.—Commercially available $SnCl_4$ (Riedel-de Haen, 99%), $NaBH_4$ (Fluka), 1,10-phenanthroline (Nacalai Tesque), synthetic graphite (Timcal KS6, 19 m^2/g), and methanol (Merck) were used as received without further purification. Deionized water was purified by double distillation.

Synthesis of 10 nm Sn nanoparticles and Sn-KS6 nanocomposites.—5 mL of 0.1 M $SnCl_4$ aqueous solution was added to a suspension of 0.1 g of 1,10-phenanthroline (phen) in 5 mL of water (phen: $SnCl_4$ = 1:1). A clear solution was obtained after stirring for a few minutes, indicating the formation of the coordination compound (phen)$SnCl_4$.[22] 20 mL of 0.1 M $NaBH_4$ aqueous solution was then introduced dropwise ($NaBH_4$: (phen)$SnCl_4$ = 4:1). The mixture turned red, indicating the formation of a sol of phen-capped Sn nanoparticles. The hydrosol was further stirred for 2 h before the Sn nanoparticles were spun down in an ultracentrifuge (15,000 rpm for 1 h). The solid product recovered as such was washed with water and methanol, and vacuum dried at 400 K. For the preparation of Sn-graphite composites, a calculated amount of synthetic graphite KS6 was added to the (phen)$SnCl_4$ solution right at the start. The suspension was sonicated for 1 h before the addition of the reducing agent $NaBH_4$.

Synthesis of 3.5 nm Sn nanoparticles and Sn-KS6 nanocomposites.—Smaller Sn nanoparticles could be obtained by adding 10 mL of 0.05 M $SnCl_4$ instead of 5 mL of 0.1 M $SnCl_4$ to the suspension of 0.1 g of phen in 10 mL of water. The color of the resulting Sn hydrosol was pale yellow.

Electrochemical measurements.—A *N*-methyl pyrrolidinone (NMP) slurry containing 80 wt % of the Sn-graphite powder (various samples), 10 wt % each of conductive carbon black (Super-P)

* Electrochemical Society Student Member.
** Electrochemical Society Active Member.
z E-mail: cheleejy@nus.edu.sg

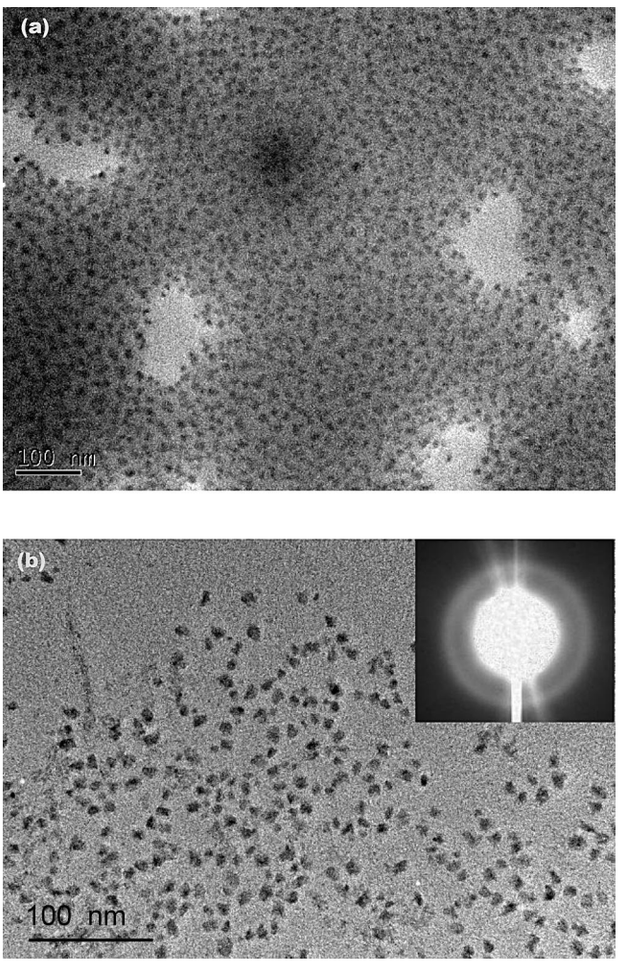

Figure 1. TEM image of as-prepared 7-13 nm Sn nanoparticles (a) dispersed in a single phen matrix and (b) after the removal of the phen matrix.

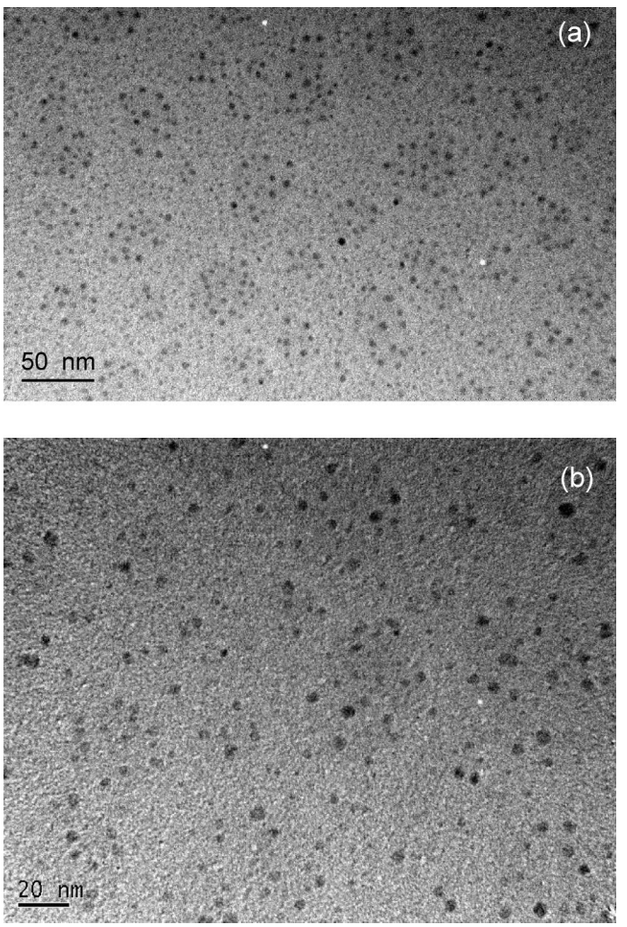

Figure 2. TEM images of 2-5 nm Sn nanoparticles at different magnification scales.

and polyvinylidene fluoride (Aldrich) was uniformly applied to a copper foil (0.7 mm). The coated foil was cut into disk electrodes 11 mm in diameter. The electrodes were vacuum dried overnight at 400 K followed by compression at 2.0×10^6 Pa. They were then assembled into Li test cells using 0.75 mm lithium foil as the negative electrode, microporous polypropylene separators, and an electrolyte of 1 M $LiPF_6$ in a 50:50 w/w mixture of ethylene carbonate (EC) and diethyl carbonate (DEC). Cell assembly was carried out in a recirculating argon glove box where both the moisture and oxygen contents were below 1 ppm each. All cells were tested at a constant current density of 0.4 mA/cm^2 and were charged (Li^+ insertion) and discharged (Li^+ extraction) between fixed voltage limits (5 mV-2 V) on a Maccor series 2000 battery tester.

Materials characterizations.—Transmission electron microscope (TEM) images were obtained from a JEOL JEM-2010 microscope. Powder XRD was carried out on a Siemens D6000 diffractometer. X-ray photoelectron spectra (XPS) were collected by a KRATOS AXIS His. UV-visible spectra were recorded by a Shimadzu UV-3101 PC double-beam spectrophotometer. FTIR spectra were obtained on a BIO-RAD FTS 135 FTIR spectrophotometer using the KBr pellet method.

Results and Discussion

Tin particles (larger than 1 μm) could be easily obtained by adding $NaBH_4$ to a $SnCl_2$ aqueous solution.[18] This process is not suitable for producing nanoparticles because the addition of a strong reducing agent ($NaBH_4$) rapidly changes the reaction environment, making it difficult to control the nucleation and growth of the particles. However, in the presence of a complexing agent or a surface passivating ligand (*e.g.*, citrate ions which coordinate to the metal surface through the COO^- group), 100-300 nm Sn particle could be formed by this simple reductve process.[18] A brief survey of the literature shows that polyvinylpyrrolidone (PVP) is one of the most popular surface passivating agent used in metal nanoparticle preparations.[23,24] Our attempt to prepare Sn nanoparticles protected by PVP was unsuccessful as the resulting nanoparticles showed heavy agglomeration. Hence the use of 1,10-phenanthroline (phen), a Lewis base, to inhibit the agglomeration of nanoparticles was explored. Unlike polymers, such as PVP which stabilizes through multisite adsorption of the polymer on the nanoparticles after the latter are formed, phen is able to bond to Sn in the $SnCl_4$ precursor stage as a coordinating complex.[22] This should in principle reduce the reactivity of Sn in chemical reactions, and a more homogenous reaction environment for chemical reduction may then be established. In addition, once the Sn particles are formed, they are instantly coordinated to phen by the pair of chelating nitrogen donor sites adjoining the two fused heterocyclic aromatic rings.[25] The capping of the Sn nanoparticles prevents further growth of the nanoparticles and is expected to control the growth rate much more effectively than PVP.

Figure 1a shows a typical TEM image of phen-capped Sn nanoparticles (average particle size of 10 nm) on a TEM grid, which had been washed in deionized water and dried at 400 K in vacuum. A large number of Sn nanoparticles of almost the same size were

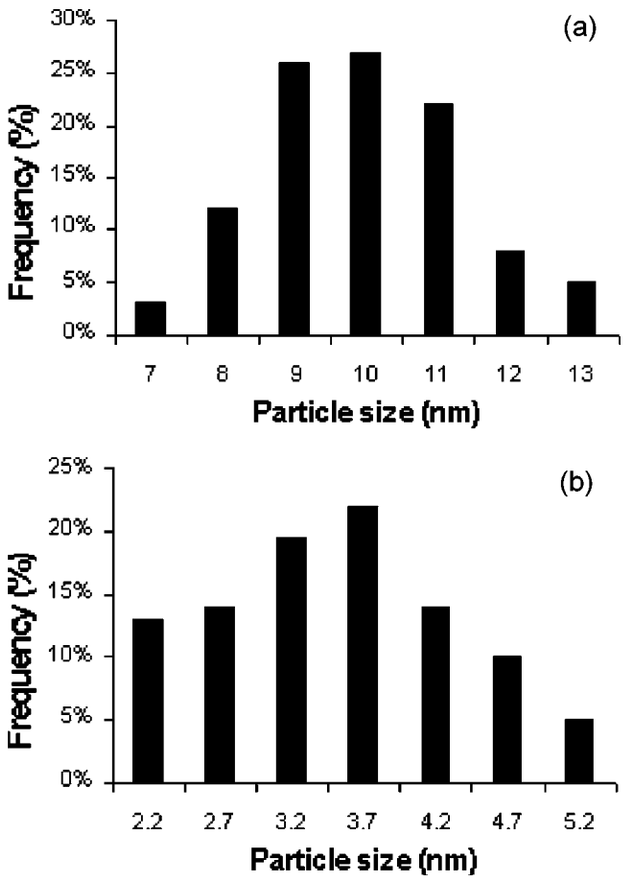

Figure 3. Particle size distribution from TEM measurements for (a) 10 nm Sn nanoparticles and (b) 3.5 nm Sn nanoparticles.

found embedded in a web of phen molecules, which coordinated strongly with one other and with the Sn nanoparticles possibly through surface adsorption. After the TEM grid was washed with methanol, in which phen is readily soluble, the phen domains disappeared and only the nanoparticles were left behind (Fig. 1b). Measurements based on these TEM images revealed that the Sn nanoparticles were nearly monosized with an average particle size of

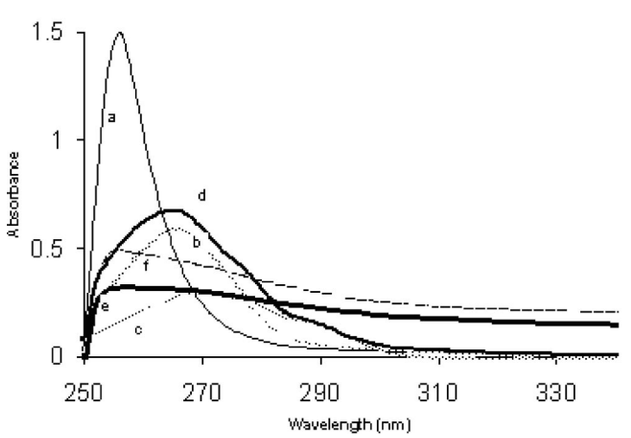

Figure 4. UV/visible absorption spectra of (a) $SnCl_4$, (b) phen, (c) (phen)$SnCl_4$, (d) phen-capped Sn nanoparticles, (e) 10 nm Sn particles, and (f) standard (100 nm) Sn particles.

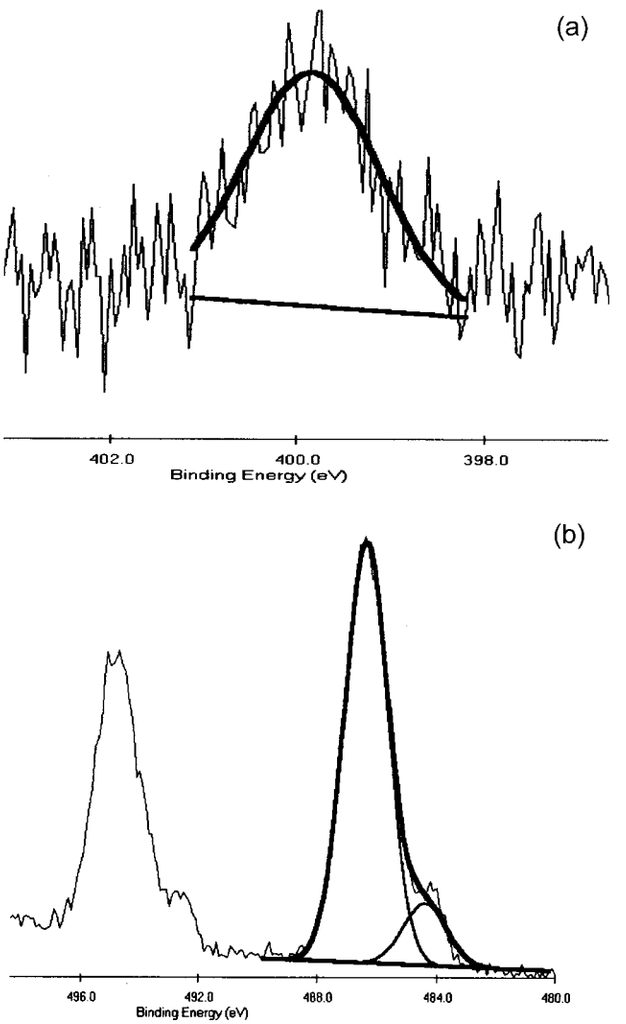

Figure 5. XPS of phen-capped 10 nm Sn particles in the (a, top) N 1s region and (b, bottom) the Sn $3d_{5/2}$ region.

10.0 nm and a standard deviation of 1.7 nm, and were well separated from one another.

Sn nanoparticles of even smaller sizes and a narrower size distribution were obtained by using a more dilute solution of (phen)$SnCl_4$. The TEM images in Fig. 2a and b show nanoparticles with a mean particle size of 3.5 nm and a standard deviation of 0.8 nm. The nanoparticles were uniformly distributed without any noticeable agglomeration both inside and outside of the phen domains. A histogram of particle size distribution based on TEM measurements is given in Fig. 3 for the two batches of Sn nanoparticles of average particle sizes of 10 and 3.5 nm, respectively. The statistics were generated by counting approximately 250 particles. The experimental observation of a lower (phen)$SnCl_4$ concentration aiding in the formation of smaller and more uniform Sn nanoparticles corroborates the slow kinetics in the particle formation process described earlier.

In contrast to the procedure in Ref. 19, the approach mentioned in this study does not require the handling of air-sensitive and unstable compounds such as $[Sn(NMe_2)_2]_2$. The (phen)$SnCl_4$ precursor can be easily synthesized *in situ*. Its stability in air makes it possible to produce Sn nanoparticles under the ambient conditions in an aqueous system. It should be emphasized that compared to the previous effort,[19] smaller Sn nanoparticles with a narrower size dis-

tribution are obtained here, and with almost no particle agglomeration.

Figure 4 shows the absorption spectra of (a) $SnCl_4$, (b) phen, (c) (phen)$SnCl_4$, (d) phen stabilized Sn nanoparticles, (e) pristine Sn nanoparticles, and (f) commercially available Sn nanoparticles (100 nm, Aldrich). The absorption maxima of (phen)$SnCl_4$ precursor,[22] was located at a higher wavelength compared to $SnCl_4$ and phen. Upon the addition of $NaBH_4$, the (phen)$SnCl_4$ peak at 270 nm disappeared signalling the complete reduction from Sn^{4+} to Sn^0. In addition, UV-visible spectra of obtained Sn nanoparticles showed mostly the UV absorption features of phen, which is taken to indicate the presence of remnants of phen on the Sn nanoparticle surface. UV-visible spectra were also collected after washing the phen-stabilized Sn nanoparticles with methanol and the results were indistinguishable from the commercially available Sn nanoparticles, and without any UV-visible signature of phen. FTIR measurements also agreed well with these results. The coordination compound (phen)$SnCl_4$ exhibited a number of sharp peaks (1590, 1539, 1428, 1150, 856, 717 cm^{-1}) which could be attributed to the phen ligand. Peaks at 1559, 1536, 1424, 852 cm^{-1} remained visible for the phen-Sn nanoparticles before washing, indicating again the presence of phen on the nanoparticle surface. Comparable FTIR in the spectra of (phen)$SnCl_4$ and phen-stabilized Sn were shifted to slightly higher wavenumbers relative to phen, possibly as a result of the coordination of phen to $SnCl_4$ or to the Sn nanoparticles.[25]

The presence of the N 1s signal in the XPS spectrum of the prepared Sn nanoparticles further confirmed the adsorption of phen on the nanoparticle surface (Fig. 5a). Combining the results from TEM imaging, UV-visible spectroscopy and FTIR spectroscopy, it could be postulated that the phen molecules coordinated strongly with Sn to provide an extensive surface coverage on the Sn nanoparticles. A similar effect of strongly coordinating ligands was previously observed for phen-stabilized Pd nanoparticles.[26]

Based on these observations, we propose that the role of 1,10-phenanthroline as follows (Scheme I): phen promotes the formation of the coordination compound (phen)$SnCl_4$,[22] The formation of a coordination compound between the ligand and the metal at the precursor level (phen and $SnCl_4$ in this case) could potentially offer better control in the nucleation and growth of the nanoparticles. This advantage was largely overlooked in the current procedures for preparing ligand-stabilized nanoparticles. For example, PVP-protected Ag nanoparticles were prepared by the reduction of $AgClO_4$.[24] As there is no affinity between PVP and $AgClO_4$ at the precursor level, there is minimal control in nucleation besides the steric effects of PVP. Particle growth control that depends on the interactions between PVP and the nanoparticles only comes in after the nanoparticles are formed.

The Sn 3d peak in the XPS spectrum of the Sn nanoparticles (Fig. 5b) appeared as a doublet with a separation of 8.5 eV. Deconvolution of the Sn $3d_{5/2}$ signal indicated the presence of two species with binding energies of 484.7 and 486.4 eV in the ratio of 1:6.7, most likely due to Sn and SnO or SnO_2, respectively (SnO and SnO_2 have experimentally indistinguishable binding energies).[19] This is an indication of the surface oxidation of the Sn nanoparticles. It is indeed common for metal nanoparticles to form a metal oxide shell under ambient conditions. A similar observation was also re-

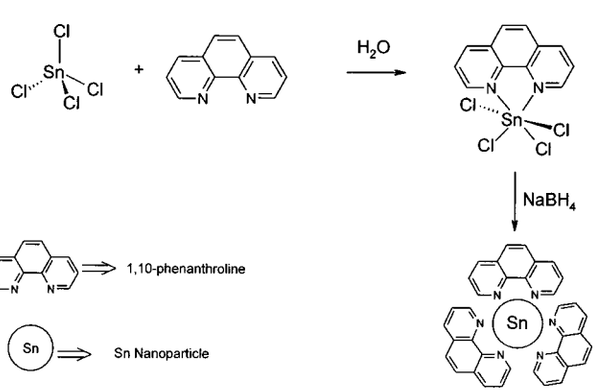

Scheme 1. Proposed reaction scheme for the preparation of phen-capped Sn nanoparticles.

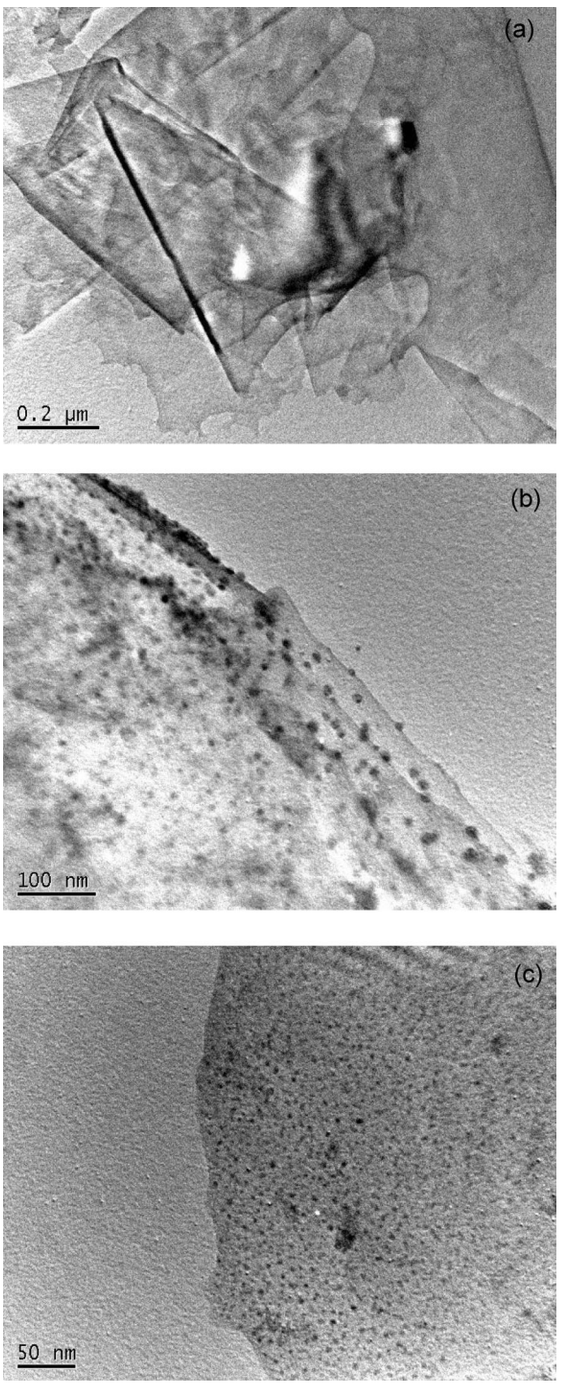

Figure 6. TEM images of (a) pristine KS6, (b) 18.7 wt % Sn (10 nm)-KS6 nanocomposites, and (c) 19.8 wt % Sn (3.5 nm)-KS6 nanocomposites.

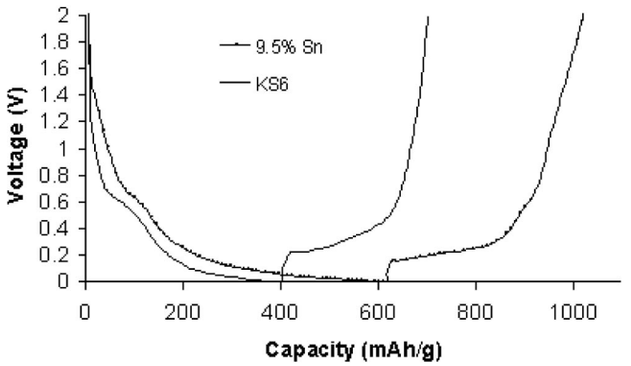

Figure 7. The first cycle lithiation and delithiation of graphite and 9.5 wt % Sn (10 nm)-graphite.

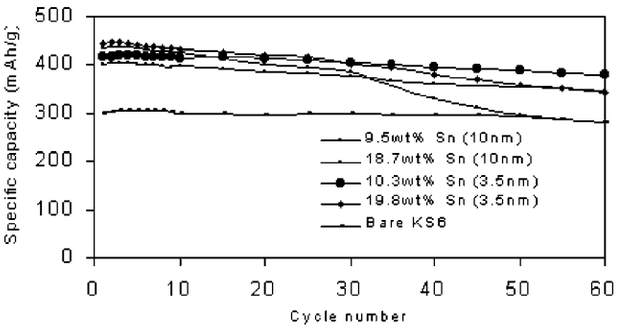

Figure 8. Cyclability of various Sn-modified graphite composite anodes (0.4 mA/cm^2, 5 mV-2V).

ported for the Sn nanoparticles obtained in Ref. 19. The surface oxide is likely to be SnO or SnO_2, which hinders further oxidation. SnO_2 nanoparticles, a wide bandgap n-type semiconductor material, could be formed after prolonged heating of the Sn nanoparticles.

Selected area electron diffraction (SAED) of the Sn nanoaprticles (inset of Fig. 1b) showed the characteristic ring pattern of an amorphous material. XRD also confirmed that the Sn nanoparticles were X-ray amorphous even after heating to 450 K in vacuum (the melting point of Sn is 505 K). Amorphous Sn has been found to have better cyclability compared to the crystalline polymorph.[27]

Figure 6a shows the TEM image of pristine KS6. Synthetic graphite KS6 with a flake size of 1-5 μm is a reasonably good electron conductor and a good Li host (only 6% volume change in Li-ion intercalation and deintercalation reactions), and hence its addition to Sn would not diminish the overall capacity in the way an active-inactive domain system would.[7,8] The TEM images in Fig. 6b and c show, respectively, the uniform distribution of 18.7 wt % Sn (10 nm) and 19.8 wt % Sn (3.5 nm) nanoparticles on the graphite surface for the Sn-graphite nanocomposites prepared in the way described in the experimental section. A large number of Sn nanoparticles were located on the surface of KS6, the edges of the graphite flakes could be seen clearly and no nanoparticles were found outside of graphite. The uniform dispersion of Sn without aggregation led us to hypothesize that there are active sites on the graphite surface, which help to bind and stabilize the nanoparticles.

Elemental analysis by inductively coupled plasma spectroscopy (ICPS) showed Sn (3.5 nm) loadings of 10.3 wt %, 19.8 wt %, and Sn (10 nm) loadings of 9.5 wt % and 18.7 wt % in four samples of (phen)$SnCl_4$-derived Sn-KS6 composites. The first cycle charging (Li insertion) and discharging (Li extraction) curves of 9.5 wt % Sn(10 nm)-KS6 composite and pristine graphite (KS6) are shown in Fig. 7. Cycling was performed at a constant current density of 0.4 mA/cm^2 (approximating the C/6 rate) with cutoff potentials at 5 mV and 2V *vs.* Li/Li$^+$. Discharge and recharge capacities of 618 and 402 mAh/g, respectively, were obtained in the first cycle, resulting in a 65% coulombic efficiency. This value is an improvement over our previous results (~60-62%) of SnO_2-KS6 nanocomposites.[16,17] When SnO_2 is involved, there is an additional mechanism for irreversible capacity loss due to the decomposition of SnO_2 into Li_2O and Sn at 1 V and above in the first lithiation cycle as shown in Eq. 1 below

$$SnO_2 + 4Li + 4e^- \rightarrow 2Li_2O + Sn \qquad [1]$$

Subsequent to the metallic Sn formation reaction, Li$^+$ insertion and extraction reactions would then proceed reversibly via Eq. 2

$$Sn + xLi + xe^- \rightleftarrows Li_xSn \quad (x_{max} = 4.4) \qquad [2]$$

If Sn is used as the Li storage compound, the first reaction is not expected to occur and the coulombic efficiency should be, in principle, increased. The Sn nanoparticles in the Sn-graphite composites actually had a core shell structure of the type Sn-SnO or Sn-SnO_2 because of the facile oxidation of the Sn surface. Hence the irreversible capacity loss due to decomposition of tin oxides could not be completely eliminated. The core-shell structure, on the other hand, could be of special interest and advantageous to lithium-ion battery applications. This is because the Li_2O formed in the decomposition of SnO or SnO_2 in the first lithiation cycle is known to help restrain the pulverization of Sn particles during applications.[5] Hence a moderate presence of SnO or SnO_2 would benefit from the Li_2O existence without an unduly large irreversible capacity loss.

The cycling performance of a series of Sn-KS6 composites (10.3 and 19.8 wt % of 3.5 nm Sn, and 9.5 and 18.7 wt % of 10 nm Sn) is compared in Fig. 8. Generally, an increase in the amount or the size of the Sn nanoparticles led to poorer electrode cyclability. For the sample with 10.3 wt % of Sn (3.5 nm), discharge capacities of 415 and 379 mAh/g were obtained in the first and the 60th cycle,

Table I. Cyclability of various Sn-graphite and SnO_2-graphite nanocomposites.

Samples	Initial specific capacity (mAh/g)	Initial efficiency (%)	Capacity retained at cycles (%)			
			10	30	40	60
9.8 wt % SnO_2 (17 nm)[16]	384	61.5	99.4	96.3	94.7	-
16.5 wt % SnO_2 (17 nm)[16]	428	60.5	99.2	90.1	82.5	-
9.2 wt % SnO_2 (5 nm)[17]	404	62.5	98.4	90.7	82.3	-
14.5 wt % SnO_2 (5 nm)[17]	462	59.7	97.2	83.6	72.3	-
10.3 wt % Sn (3.5 nm)	415	65.5	99.7	97.3	95.1	91.3
19.8 wt % Sn (3.5 nm)	442	63.8	97.7	90.5	85.9	76.9
9.5 wt % Sn (10 nm)	402	65.0	98.7	93.8	90.0	85.8
18.7 wt % Sn (10 nm)	434	64.2	97.9	89.2	76.0	64.9
Pristine KS6	300	74.1	100	99.1	98.3	93.8
Pristine Sn or SnO_2	~600-700	~40-60	-	-	-	-

respectively. In other words, 91.3% of the initial capacity could be retained after 60 cycles, which was only marginally lower than the retention value of pristine KS6 (93.8%) in the same number of cycles. We are not aware of any other report of Sn-C composites showing such high cyclability. The good cyclability of Sn-KS6 nanocomposites prepared by the current method is believed to be a combination of the uniform distribution of nonagglomerating small Sn particles on the graphite surface and the successful control of the volume changes in Li-Sn reactions.

The Sn-KS6 composites showed distinctively better performance than what was expected from a physical mixture of two independent components. For example, the discharge capacity (415 mAh/g) of 10.3 wt % Sn-KS6 is higher than the weighted sum of the discharge capacities of graphite (300 mAh/g)[16] and theoretical capacity of Sn (990 mAh/g)[15] (usually the realizable discharge capacities of Sn or SnO_2 are around 600-700 mAh/g).[9,18] It is, however, not clear whether one could (or should) partition the observed nanocomposite capacities between their constituents. As a first approximation, the small capacity loss after 60 cycles could be attributed to mostly Sn nanoparticles. The agglomeration of Sn nanoparticles appears to be an inevitable event after prolonged cycling of the electrode.[28,29]

Relative to the 10.3 wt % Sn (3.5 nm) sample, the 19.8 wt % Sn (3.5 nm)-KS6 composite had an expectedly higher capacity (442 mAh/g) due to the increase in the tin content, but capacity fading was also more pronounced with 23.1% of the initial capacity lost in 60 cycles. This was most likely due to the increase in the rate and the extent of Sn particle agglomeration in composites with higher tin contents. For the composites containing 9.5 and 18.7 wt % of 10 nm Sn, the initial capacities were 402 and 434 mAh/g, respectively, 85.8 and 64.9% of which could be retained after 60 cycles. The stronger capacity fading in 10 nm Sn nanocomposites clearly indicates the advantage of using smaller nanoparticles. In addition, the 3.5 nm Sn nanoparticles were also more monodispersed than the 10 nm Sn nanoparticles. Therefore a uniform distribution of smaller Sn nanoparticles would lead to a more homogenous volume change during Li^+ insertion and extraction reactions, which is easier for graphite to buffer.

Table I compares the electrochemical properties of the Sn-KS6 prepared here with our previous work[16,17] on SnO_2-KS6 nanocomposites prepared by a variety of different methods. The following conclusions can be drawn from such a comparison: (*i*) Sn-graphite nanocomposites generally show the expected higher coulombic efficiencies than SnO_2-graphite nanocomposites, (*ii*) all samples with lower Sn or SnO_2 contents show improved cyclabilities than those with higher contents. Capacity fading becomes noticeable when the Sn or SnO_2 content is increased from 9 to around 16 wt %, indicating that the range for optimal Sn or SnO_2 loading is rather limited. Even when Sn or SnO_2 particles are small and uniformly distributed, a large number these particles would not be able to deliver high capacity concurrently with good cyclability. (*iii*) The table also shows that the 5 nm SnO_2 nanoparticles actually displays more severe capacity fading than samples containing larger SnO_2 (17 nm) and Sn (10 nm) particles. The particles size alone is therefore a necessary but insufficient condition to assure good cyclability. It is rather the combination of small particle size, uniform particle size distribution, and low particle concentration that is important to cyclability preservation. The 10.3 wt % Sn (3.5 nm) nanocomposite excelled because it possessed all of these desirable attributes. This should not come as a surprise as it is common knowledge that the properties of nanoparticle systems are strongly dependent on both particle size and particle size distribution.[30]

Conclusion

In conclusion, Sn nanoparticles about 10 and 3.5 nm in size and Sn-graphite nanocomposites were prepared from an *in situ* formed $(phen)SnCl_4$ precursor. The phen ligand stabilizes the nanoparticles against agglomeration during preparation and the dispersion of the nanoparticles in graphitic carbon inhibits particle agglomeration during applications. In principle, phen could also be useful as a protective agent in the preparation of other metal nanoparticles. The 10.3 wt % 3.5 nm Sn-graphite nanocomposite prepared as such displayed a high reversible Li^+ storage capacity of 415 mAh/g, of which 91.3% could be retained after 60 charge and discharge cycles. This is a significant improvement over previous efforts on Sn-based graphite composites reported in the literature. Particle size and particle size distribution are both very important factors determining the applicability of Sn-based nanoparticles in Li-ion batteries.

The Singapore-MIT alliance, National University of Singapore, assisted in meeting the publication costs of this article.

References

1. Y. Idota, A. Matsufuji, Y. Mackawa, and T. Miyasaki, *Science*, **276**, 1395 (1997).
2. O. Mao, R. L. Turner, I. A. Courtney, B. D. Fredericksen, M. I. Buckett, L. J. Krause, and J. R. Dahn, *Electrochem. Solid-State Lett.*, **2**, 3 (1999).
3. I. A. Courtney, W. R. McKinnon, and J. R. Dahn, *J. Electrochem. Soc.*, **146**, 59 (1999).
4. A. Ulus, Y. Rosenberg, L. Burstein, and E. Peled, *J. Electrochem. Soc.*, **149**, A635 (2002).
5. J. Yang, Y. Takeda, N. Imanishi, and O. Yamamoto, *J. Electrochem. Soc.*, **146**, 4009 (1999).
6. N. Li and C. Martin, *J. Electrochem. Soc.*, **148**, A164 (2001).
7. J. Y. Lee, R. F. Zhang, and Z. L. Liu, *Electrochem. Solid-State Lett.*, **3**, 167 (2000).
8. J. Y. Lee, R. F. Zhang, and Z. L. Liu, *J. Power Sources*, **90**, 70 (2000).
9. J. Read, D. Foster, J. Wolfenstine, and W. Behl, *J. Power Sources*, **96**, 277 (2001).
10. G. X. Wang, J. H. Ahn, M. J. Lindsay, L. Sun, D. H. Bradhurst, S. X. Dou, and H. K. Liu, *J. Power Sources*, **97-98**, 211 (2001).
11. M. Egashira, H. Takatsuji, S. Okada, and J. Yamaki, *J. Power Sources*, **107**, 56 (2002).
12. J. K. Lee, D. H. Ryu, J. B. Ju, Y. G. Shul, B. W. Cho, and D. Park, *J. Power Sources*, **107**, 90 (2002).
13. B. Veeraraghavan, A. Durairajan, B. Haran, B. Popov, and R. Guidotti, *J. Electrochem. Soc.*, **149**, A675 (2002).
14. Y. Liu, J. Y. Xie, Y. Takeda, and J. Yang, *J. Appl. Electrochem.*, **32**, 687 (2002).
15. H. Li, Q. Wang, L. H. Shi, L. Q. Chen, and X. J. Huang, *Chem. Mater.*, **14**, 103 (2002).
16. Y. Wang, J. Y. Lee, and B. H. Chen, *Electrochem. Solid-State Lett.*, **6**, A19 (2003).
17. Y. Wang and J. Y. Lee, *Electrochem. Commun.*, **5**, 292 (2003).
18. J. Yang, M. Wachtler, M. Winter, and J. O. Besenhard, *Electrochem. Solid-State Lett.*, **2**, 161 (1999).
19. C. Nayral, T. Ould-Ely, A. Maisonnat, B. Chaudret, P. Fau, L. Lescouzere, and A. Peyre-Lavigne, *Adv. Mater. (Weinheim, Ger.)*, **11**, 61 (1999).
20. A. Stella, M. Nisoli, S. De Silvestri, O. Svelto, G. Lanzani, P. Cheyssac, and R. Kofman, *Phys. Rev. B*, **53**, 15497 (1996).
21. T. Bachels and H. J. Guntherodt, *Phys. Rev. Lett.*, **85**, 1250 (2000).
22. V. J. Hall and E. R. T. Tiekink, *Z. Kristallogr.*, **211**, 47 (1996).
23. J. S. Bradley, J. M. Millar, and E. W. Hill, *J. Am. Chem. Soc.*, **113**, 4106 (1991).
24. I. P. Santos and L. M. L. Marzan, *Langmuir*, **18**, 2888 (2002).
25. T. Trindade, P. O'Brien, and X. M. Zhang, *Chem. Mater.*, **9**, 523 (1997).
26. N. Toshima, Y. Shiraishi, T. Teranishi, M. Miyake, T. Tominaga, H. Watanabe, W. Brijoux, H. Bonneemann, and G. Schmid, *Appl. Organomet. Chem.*, **15**, 178 (2001).
27. J. J. Zhu, Z. H. Lu, S. T. Aruna, D. Aurbach, and A. Gedanken, *Chem. Mater.*, **12**, 2557 (2000).
28. H. Li, X. J. Huang, L. Q. Chen, Z. G. Wu, and Y. Liang, *Electrochem. Solid-State Lett.*, **2**, 547 (1999).
29. H. Li, L. H. Shi, W. Lu, X. J. Huang, and L. Q. Chen, *J. Electrochem. Soc.*, **148**, A915 (2001).
30. I. S. Armadi, Z. L. Wang, T. C. Green, A. Henglein, and M. A. El-Sayed, *Science*, **272**, 1924 (1996).